NeuroImage: Clinical 1 (2012) 18–28

Contents lists available at ScienceDirect

NeuroImage: Clinical

journal homepage: www.elsevier.com/locate/ynicl

Computational analysis reveals increased blood deposition following repeated mild traumatic brain injury ☆

Virginia Donovan [a,b], Anthony Bianchi [c], Richard Hartman [d], Bir Bhanu [c], Monica J. Carson [a,b,e], Andre Obenaus [a,b,f,*]

[a] Cell, Molecular and Developmental Biology Program, University of California, Riverside, 1140 Bachelor Hall, Riverside, CA 92521, USA
[b] Center for Glial-Neuronal Interactions, University of California, Riverside, School of Medicine Research Building, CA 92521, USA
[c] Center for Research in Intelligent Systems, University of California, Riverside, 216 Winston Chung Hall, Riverside, CA 92521, USA
[d] Department of Psychology, Loma Linda University, 11130 Anderson St. #119, Loma Linda, CA 92354, USA
[e] Division of Biomedical Sciences, University of California, Riverside, 1274 Webber Hall, CA 92521, USA
[f] Department of Pediatrics, Loma Linda University, Coleman Pavilion Room A1109, Loma Linda, CA 92354, USA

ARTICLE INFO

Article history:
Received 17 May 2012
Received in revised form 12 July 2012
Accepted 4 August 2012
Available online 23 August 2012

Keywords:
Edema
Hemorrhagic progression
Histogram
T2
Quantitative magnetic resonance imaging

ABSTRACT

Mild traumatic brain injury (mTBI) has become an increasing public health concern as subsequent injuries can exacerbate existing neuropathology and result in neurological deficits. This study investigated the temporal development of cortical lesions using magnetic resonance imaging (MRI) to assess two mTBIs delivered to opposite cortical hemispheres. The controlled cortical impact model was used to produce an initial mTBI on the right cortex followed by a second injury induced on the left cortex at 3 (rmTBI 3d) or 7 (rmTBI 7d) days later. Histogram analysis was combined with a novel semi-automated computational approach to perform a voxel-wise examination of extravascular blood and edema volumes within the lesion. Examination of lesion volume 1d post last injury revealed increased tissue abnormalities within rmTBI 7d animals compared to other groups, particularly at the site of the second impact. Histogram analysis of lesion T2 values suggested increased edematous tissue within the rmTBI 3d group and elevated blood deposition in the rm TBI 7d animals. Further quantification of lesion composition for blood and edema containing voxels supported our histogram findings, with increased edema at the site of second impact in rmTBI 3d animals and elevated blood deposition in the rmTBI 7d group at the site of the first injury. Histological measurements revealed spatial overlap of regions containing blood deposition and microglial activation within the cortices of all animals. In conclusion, our findings suggest that there is a window of tissue vulnerability where a second distant mTBI, induced 7d after an initial injury, exacerbates tissue abnormalities consistent with hemorrhagic progression.

1. Introduction

Traumatic brain injury (TBI) affects an estimated 1.7 million individuals and contributes to a third of injury-related deaths annually in the United States, with mild TBI (mTBI) accounting for approximately 75% of all TBI cases (Corrigan et al., 2010; Faul et al., 2010; Tagliaferri et al., 2006). Comparison of clinical computed tomography (CT) and magnetic resonance imaging (MRI) scans found that MRI allows for increased detection of mTBI related abnormalities (Lee et al., 2008). However given the standardized definition of mTBI wherein there are no observable changes on standard MRI, new approaches are warranted to assess mTBI from neuroimaging data (VA/DoD, 2009).

Standard MRI, such as T1 and T2 weighted imaging (T1WI, T2WI), of mTBI results in low contrast subtle tissue changes that create difficulty in evaluation and detection of mild injury. As a result, enhanced MRI quantification methods are needed to identify and monitor the progression of mild injuries. Currently, quantitative semi-automatic MRI analysis of moderate to severe experimental TBI has been used to investigate tissue pathology (Immonen et al., 2009; Irimia et al., 2011; Kharatishvili et al., 2009). In these experimental models, manually defined regions of interest revealed positive correlations between T2 relaxation values and poor histological and behavioral outcomes (Immonen et al., 2009; Kharatishvili et al., 2009). However, little work has been done using models of mTBI. One study in which an automated method of whole brain MRI analysis was developed, demonstrated increased abnormal gray matter within the first 5 h following experimental mild and severe TBI (Colgan et al., 2010). However, long-term (days, weeks) quantitative

Abbreviations: DTI, diffusion tensor imaging; FA, fractional anisotropy; HPC, hemorrhagic progression of the contusion; MD, mean diffusivity.

* Corresponding author at: Department of Pediatrics, Loma Linda University, 11175 Campus Street, Rm A1120, Loma Linda, CA 92354, USA. Tel.: +1 909 558 7801; fax: +1 909 558 7519.
E-mail address: aobenaus@llu.edu (A. Obenaus).

2213-1582/$ – see front matter © 2012 The Authors. Published by Elsevier Inc. All rights reserved.
http://dx.doi.org/10.1016/j.nicl.2012.08.001

computational MRI analysis of the evolution of neuropathology following mild injuries, and in particular repeated injury, remains unexplored.

One of the many consequences of TBI is microvascular dysfunction, which can result in tissue ischemia, edema and hemorrhagic progression (Kurland et al., 2012). Depending on the type and severity of brain injury, peak edema is typically observed 24–48 h following injury and resolves by approximately 4–7 days, while hemorrhagic lesions can occur within the first 3–4 days and resolution can take months (Kurland et al., 2012; Obenaus et al., 2007; Oehmichen et al., 2003). Hemorrhagic progression of a contusion (HPC) is the expansion of an existing or the development of a new hemorrhagic lesion (Simard et al., 2010). HPC is observed clinically in mild to severe cases of TBI and substantially increases tissue damage, as blood is particularly neurotoxic (Alahmadi et al., 2010; Kurland et al., 2012; Sifri et al., 2004, 2006; Simard et al., 2010; Xue and Del Bigio, 2000). Experimental modeling has demonstrated that vessel fragmentation plays a key role in HPC development and blocking these cellular cascades results in decreased necrotic tissue volume and improved behavioral outcomes (Simard et al., 2009).

Most patients who sustain an mTBI appear to recover normally from the injury, though there is evidence that sustaining multiple mTBIs can result in cumulative detrimental effects (Belanger et al., 2010). However little is known about the underlying pathology and long-term consequences of repeated mTBI (rmTBI). Animal models where induction of two injuries to the same location was performed demonstrated a window of vulnerability of approximately 1–5 days following an mTBI, in which a second impact can result in increased lesion volume, axonal injury and inflammation (Laurer et al., 2001; Longhi et al., 2005; Shitaka et al., 2011). However two mTBIs 7 days apart did not result in exacerbation of injury (Longhi et al., 2005). Additional models of rmTBI in which four or five injuries to the same location were rapidly induced (24 h apart) demonstrated persistent neurological deficits with no overt cell death or blood brain barrier disruption (DeFord et al., 2002; Kane et al., 2012; Shultz et al., 2012). Surprisingly, all of the reported models of rmTBI had repeated injuries to the same anatomical location and what remains to be elucidated are the effects of multiple injuries to different brain locations.

The objective of our study was to evaluate whether the ongoing neuropathology from an initial mTBI was altered by a second contralateral injury induced 3 or 7 days later. A secondary objective was to assess the ability of computational analysis of the mTBI injury to provide quantitative information about the progression of neuropathology. We hypothesized that injuries induced 3d apart would result in larger lesion volumes at the site of the second injury, while little or no change in lesion volume was expected within groups receiving impacts 7d apart.

2. Methods

Protocols were in compliance with federal regulations and approved by the Loma Linda University Animal Health and Safety Committees.

2.1. Mild traumatic brain injury

Fifty adult male Sprague Dawley rats ages 2–4 months were randomly assigned to three experimental groups: Single mTBI and repeated mTBI induced either 3 (rmTBI 3d) or 7 (rmTBI 7d) days apart (Fig. 1A). A mild controlled cortical impact (mCCI) was used to induce mTBI as previously described (Obenaus et al., 2007), with minor modifications. Briefly, anesthetized rats (Isoflurane: 3% induction, 1–2% maintenance) were secured into a stereotactic frame and a midline incision exposed the skull surface. A craniectomy (5 mm diameter) was performed over the right hemisphere 3 mm posterior and 3 mm lateral from Bregma (Fig. 1B), where a mCCI (4 mm diameter tip, 0.5 mm depth, 6.0 m/s speed, 200 ms dwell) was delivered to the cortical surface using an electromagnetically driven piston (Leica Biosystems Inc., Richmond, IL). Animals within the rmTBI groups received a second craniectomy and mCCI on the opposite (left) cortical surface (identical Bregma coordinates) 3 or 7 days after the first mCCI (Fig. 1A, B). At the end of each surgery a sterile nylon flap (~1 cm^2) was placed over the craniectomy and the incision was closed.

2.2. MRI data collection

Animals were anesthetized (isoflurane: 3% induction, 1% maintenance) for MRI at: 1d post first injury (D1), 1d post last injury (D1 Singles, D4 rmTBI 3d, D8 rmTBI 7d), 14d post injury (D14: 14d post first, D21: 14d post last injury) and ≥60 (60–68) days post first injury (Fig. 1A). Due to imaging constraints, all MRI was performed within 24 h of the targeted time point with the exception of the rmTBI 3d group, which received imaging at 17d rather than 21d post initial injury. In vivo T2 weighted images (T2WI; TR/TE/FA = 3453 ms/20 ms/20°, 25 × 1 mm slices) and susceptibility weighted images (SWI; TR/TE/FA = 39 ms/20 ms/20°, 48 × 0.8 mm slices) were acquired with a 256 × 256 matrix using a 4.7 T Bruker Avance. SWI was used to identify extravascular blood within tissues and T2WIs were used to create T2 maps computed using in-house software (Obenaus et al., 2007).

2.3. MRI data analysis

Regions of interest (ROI), manually drawn on T2WIs using Cheshire image processing software (Hayden Image/Processing Group, Waltham, MA), included the right and left hemispheres and cortical areas containing observable abnormalities (hyper/hypo-intense signals). In a subset of animals (n = 20) transient edema was observed within the corpus callosum following the initial impact that did not expand following a second impact and quickly resolved; in this group we only assessed cortical abnormalities. For voxel-wise computational analysis of the lesions, both the ROIs and T2 maps were imported into a novel computational algorithm coded in MATLAB (MathWorks, Torrance, CA) where lesion T2 values, tissue level histograms and volumes were extracted and lesion composition was classified (Fig. 1C).

T2 value ranges for blood, edema and normal appearing brain (NAB) containing voxels were determined by taking the average T2 value of manually segregated blood and edema lesion pixels. This was performed using a training-set composed of MRI scans (6 MRI scans evaluated) collected at 1d post last injury from animals in each group that contained lesion volumes representative of the group average and contained both edema and blood. From this analysis, lesion voxels were classified as blood (<69 ms), edema (>90 ms), NAB (70–89 ms) or noise (>500 ms). Following voxel classification, a connected component analysis was performed on each slice of the brain volume in which neighboring voxels of the same class (blood, edema, NAB, and noise) were grouped (Fig. 1C). To exclude voxels with a high spatial frequency, groups were then filtered by size such that any group less than two voxels were reclassified as noise (Fig. 1C,D).

T2 histograms of the entire lesion volume were created (0–500 ms, binned into 1 ms bins) and kurtosis, skewness, mean and peak values were also calculated for each injury histogram. Total (first + second) histograms were analyzed at 1d post last injury and 14d post first injury; first and second injury histograms were analyzed at 1d post last injury and 14d post injury (first: 14d post first, second: 14d post last injury). Group histograms were normalized to the average number of pixels contributing to the lesion in order to account for differences in lesion size. A threshold of 150 pixels (approximately 2 μl of tissue) was used to reduce unnecessary noise within the data set by including only voxels clearly containing injured tissue. Histograms then underwent 2D smoothing using a low pass Gaussian filter to remove high frequency noise.

Lesion, edema and blood volumes were divided by the whole brain volume to account for differences in brain size between animals. Total lesion volumes (first + second) were analyzed from animals at 1d post last injury, 14d post first injury and at the time of final MRI (Single, rmTBI 7d: 60–68d and rmTBI 3d: 21d post first injury). First and second lesion, blood and edema volumes were analyzed at 1d

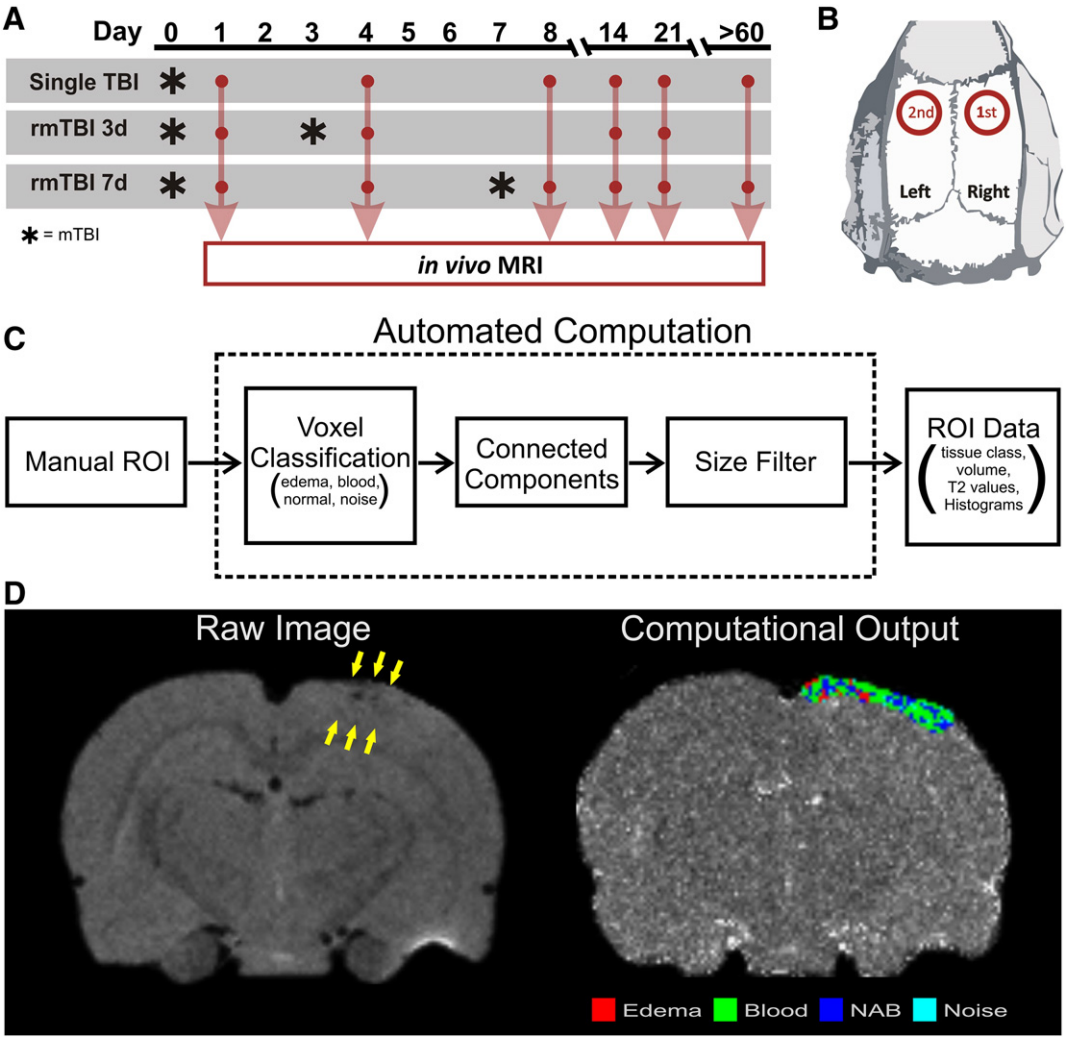

Fig. 1. Experimental design and schematic of computational analysis algorithm. A. Experimental mTBI and neuroimaging timeline. An mTBI was induced to the right cortex on D0 (denoted as an *) in all animals. The second mTBI was induced to the left cortex at either 3 or 7 days later (*). MRI was performed 1d post first (D1), 1d post last (D1 Singles, D4 rmTBI 3d, D8 rmTBI 7d) and 14d post injury (D14: 14d post first, D21: 14d post last injury) (red circles). B. Illustration of the mTBI locations for the first (right) and second (left) injuries. C. Computational schema for T2 MRI analysis to assess lesion volumes and composition for blood (<69 ms), edema (>90 ms), normal appearing brain (NAB; 70–89 ms), or noise (>500 ms) containing voxels. D. Raw T2 weighted MRI after a Single mTBI revealed observable abnormal signal intensities (yellow arrows) that were then subjected to computational analysis for tissue classification (edema, blood, NAB, noise).

post last injury and 14d post injury (first: 14d post first, second: 14d post last injury). Calculations for total (first + second), first and second lesion volumes and blood and edema volumes were performed where: a) total lesion volume was calculated by dividing the total lesion volume (first + second) by the total brain volume, b) first and second lesion volumes were calculated by dividing the first or second lesion volume by total brain volume and, c) blood and edema volumes were calculated by dividing the volume of blood or edema found in either the first or second lesion and dividing this by the respective first or second lesion volume. 3D reconstructions of lesion volumes within the brain were created using Amira software (Mercury Computer Systems, Visage Imaging, Inc., San Diego, CA, USA).

Animals with a total lesion volume (48.1–58.5 μl) greater than 4% of whole brain volume at any time point were excluded (n = 5) as this lesion size fell two standard deviations away from the average total lesion volume 1d following the initial injury and was therefore not considered a mild injury. Additionally one animal within the Single group demonstrated an increasing lesion volume over time, which was not seen in any other animals within the group and was also excluded from the study. While our study compared mild Single and repeated TBI animals, a cohort of Sham animals (n = 3) was assessed undergoing the identical experimental procedure as Single animals but without TBI. Using our computational analysis on Sham cortical ROIs, we found no significant differences ($p > 0.05$; $p = 0.82–0.95$) in blood, edema, NAB or noise volumes (μl) between the left and right cortical regions.

2.4. Tissue collection

Following the final MRI session animals were sacrificed via transcardial perfusion. Extracted brains were prepared for staining as previously described (Obenaus et al., 2007). Briefly, brains were post-fixed in 4% PFA overnight, undergoing two 30 min PBS washes following fixation. Prior to cryosectioning, brains were placed in 30% sucrose and embedded in optimal cutting temperature compound (O.T.C., Tissue Tek; Sakura Fine Tek, Torrance, CA). Coronal sections (30 μm) were collected using a Leica CM1850 cryostat (Leica Microsystems GmbH, Wetzlar Germany) and mounted directly on gelatin-chrome-alum-coated slides for histological staining (stored at −20 °C) or were free floating (stored in cryoprotectant solution at 4 °C) for immunohistochemistry.

2.5. Histochemistry

All staining was performed on slices centered under the lesion site at 14d post first injury. Prussian blue staining was performed as previously described (Obenaus et al., 2011) to detect extravascular blood within the tissue. Degenerating neurons were detected using Fluoro-Jade B (Millipore, Temecula, CA) staining on thawed tissue sections as previously described (Schmued and Hopkins, 2000).

Immunohistochemistry was performed on free floating sections as previously described (Obenaus et al., 2007). Immunolabeling was performed for astrocytes, using glial fibrillary acidic protein (GFAP; Millipore, Temecula, CA, 1:1000), and microglia, using ionized calcium binding adaptor molecule 1 (IBA1; Wako, Carpinteria, CA, 1:400). Secondary antibodies used included goat anti-mouse Alexafluor 488 (Invitrogen, Carlsbad, CA, 1:400) and goat anti-rabbit rhodamine (Millipore, Temecula, CA, 1:200). Negative controls omitted the primary antibody during the staining procedure.

The extent of blood deposition (Prussian blue) and activated microglia (IBA1) within the tissue was quantified using NIS Elements Software (Nikon Instruments Inc., Melville, NY, USA). A total of three animals (2 sections/animal), containing lesion volumes representative of the group average, were selected from each experimental group and were used to measure the medial–lateral and dorsal–ventral dispersal of blood deposition and activated microglia within the injured cortices. Activated microglia were identified based on visual signal intensity and cellular morphology as previously described (Obenaus et al., 2008).

2.6. Statistics

To correct for variability following the initial mTBI, data points were normalized to each animal's initial recorded value (current value/initial value), such that all animals received a score of 1 for the first impact. A non-parametric Kruskal–Wallis analysis of variance (ANOVA) was used for statistical analysis of the total (first + second) lesion volume as this data failed to meet the requirements of normality using a Shapiro–Wilk test. A one-tailed t-test was used to test the rmTBI 7d second lesion volume against the Single first lesion volume, as we hypothesized that the site of the second impact would have a greater injury volume than a Single injury alone. However, two-tailed t-tests were used to compare the first and second lesion volumes of all groups at 14d post injury. Further, two-tailed t-tests were used to evaluate the first and second blood and edema volumes at 1d post last injury. A p value <0.05 was considered significant ($n = 22$ Single, 4 rmTBI 3d, and 15 rmTBI 7d); error bars represent the mean ± SEM.

3. Results

3.1. Lesion composition is dependent on the interval between rmTBI

Analysis of the mTBI lesion was first evaluated using total lesion (first + second) T2 value histograms to ascertain temporal changes and identify rmTBI group differences at 1d post last injury. Compared to Singles, the rmTBI 3d animals exhibited a rightward shift in the T2 total lesion histograms suggesting increased edematous tissue that was not seen in the rmTBI 7d group (Fig. 2, top panel). In contrast, a leftward shift was observed in the rmTBI 7d lesion compared to Single animals (Fig. 2, top panel) consistent with increased blood deposition. We then further assessed each injury site independently and found that the T2 histogram at the site of the initial injury of both rmTBI groups had a leftward shift (increased blood) compared to animals receiving only a Single mTBI. However at the site of second injury, the rmTBI 3d group exhibited a dramatic shift rightward indicating increased edema, while the rmTBI 7d animals demonstrated a similar T2 profile to that observed in Single animals (Fig. 2, top panel).

At 14d post first mTBI, total brain histograms revealed a strong leftward shift in all experimental groups, demonstrating that at this sub-acute time point the edema seen at 1d post last injury had resolved. Further, the strong leftward shift of the histogram (T2 peak values: Single = 52.6 ms, rmTBI 3d = 47.8 ms, rmTBI 7d = 55.5 ms; see Table 1) in all groups suggests that extravascular blood deposition substantially contributed to the overall lesion composition at this later time point (Fig. 2, bottom panel). A closer examination of the lesion created by the initial impact revealed that all groups exhibited

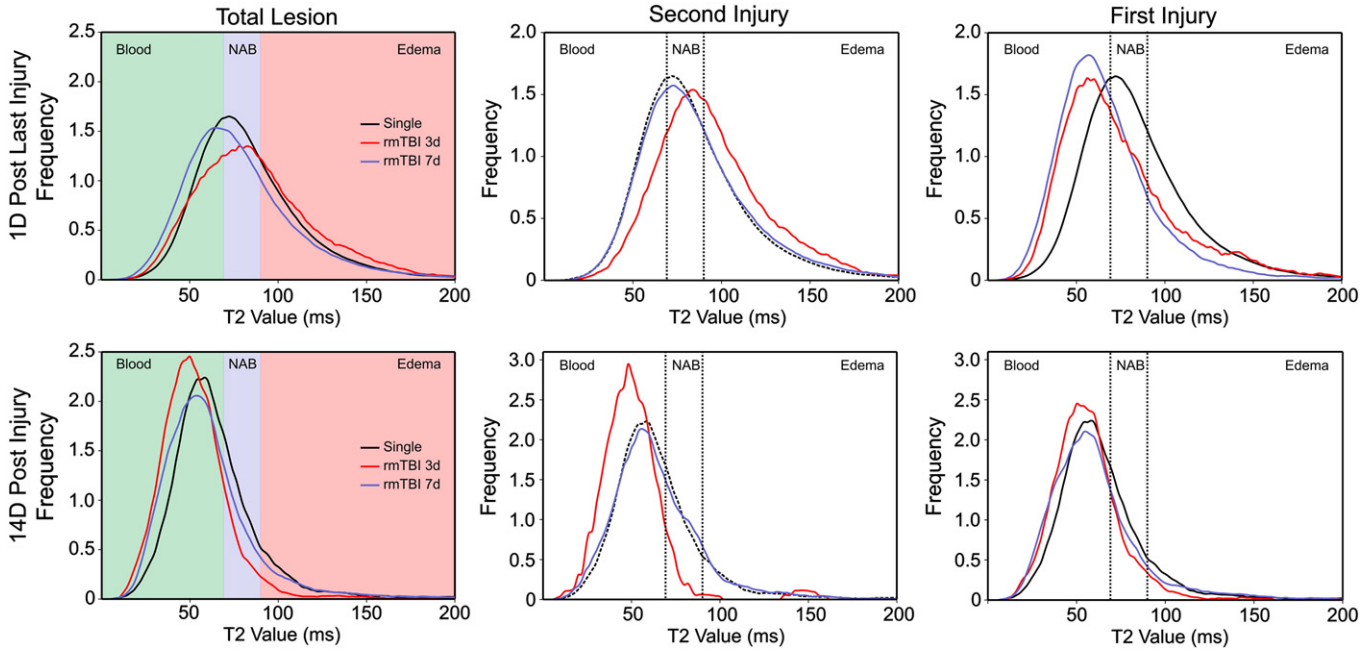

Fig. 2. Temporal shifts in T2 value distribution following rmTBI. Histograms of the total lesion (first + second) at 1d post last and 14d post injury (14d post first injury) demonstrate global changes in T2 value distribution between groups. The total lesion was then separated into the first and second lesions at 1d post last injury and 14d post injury (first: 14d post first, second:14d post last injury) to illustrate the differences in T2 distribution between the two injury sites. Color coding in the total lesion histograms illustrates the range of T2 values for tissue classification: blood (green), edema (red), or normal appearing brain (NAB; blue). Single mTBI histograms in the second injury graphs (dotted line) are those taken from the injured cortex (first injury) for comparison.

Table 1
Total lesion histogram features. Peak T2 values, mean T2 values, skewness and kurtosis measurements collected from total (first + second) lesion within Single, rmTBI 3d and rmTBI 7d groups 1d post last and 14d post first injury. Measurements ± SEM.

	Time point	Single	rmTBI 3d	rmTBI 7d	p Value
Peak T2 value (ms)	1D post last injury	70.5 ± 1.5	74.2 ± 6.1	68.3 ± 2.5	p = 0.505
	14d post first injury	52.6 ± 3.0	47.8 ± 5.4	55.5 ± 2.8	p = 0.342
Mean T2 value (ms)	1D post last injury	85.0 ± 1.4	92.6 ± 5.3[a]	78.8 ± 2.6[a]	p = 0.015
	14d post first injury	63.9 ± 2.9	55.8 ± 2.9	62.6 ± 3.0	p = 0.263
Skewness	1D post last injury	2.3 ± 0.1[a]	2.3 ± 0.3	2.9 ± 0.2[a]	p = 0.042
	14d post first injury	2.4 ± 0.2[a]	5.3 ± 0.6[a]	3.8 ± 0.7	p = 0.026
Kurtosis	1D post last injury	14.8 ± 1.2[a]	13.7 ± 2.2	21.3 ± 2.6[a]	p = 0.033
	14d post first injury	14.7 ± 1.8[a]	47.8 ± 10.4[a]	29.6 ± 7.6	p = 0.034

[a] Designates measurements that are statistically different from each other.

a similar T2 profile at 14d post first injury (Fig. 2, bottom panel). However at the second impact site, the rmTBI 3d animals demonstrated a leftward shift compared to its 1d post last injury data and the rmTBI 7d group at 14d post second injury, indicating the presence of blood and resolution of acute edema (Fig. 2, bottom panel). The site of the second impact in rmTBI 7d animals shared a similar T2 distribution to that of Singles (Fig. 2, bottom panel).

Quantitative evaluation of total lesion histogram features was undertaken (Table 1) with no significant differences in the T2 peak values between any group or time point. However, the mean histogram T2 values within the total lesion at 1d post last injury revealed a significant ($p = 0.015$) increase in T2 values within the rmTBI 3d group compared to the rmTBI 7d group (Table 1). At 14d post first injury there were no significant differences between mTBI groups. Analysis of skewness (measure of distribution asymmetry) and kurtosis (peakedness of a distribution) revealed significant differences, with the rmTBI 3d group having increased skewness ($p = 0.026$) and kurtosis ($p = 0.034$) compared to the Single group but only at the 14d post injury time point (Table 1). In contrast, the rmTBI 7d group had significant increases in skewness ($p = 0.042$) and kurtosis ($p = 0.033$) compared to Singles only at the 1d post last injury time point (Table 1).

3.2. Injury volume is dramatically increased at acute time points in rmTBI animals

The anterior–posterior extent of the mTBI injury volume was assessed computationally and included all tissue abnormalities, including blood (hypo-intense) and edema (hyper-intense) (Fig. 3A). A Single mTBI resulted in an average total brain lesion volume of 1.4 ± 0.002% of total brain volume (lesion volume approximately 15.7 ± 1.6 μl) at 1d post first injury, which appeared to have a heterogeneous mixture of blood and edema (arrowheads; Fig. 3A). Following a second mTBI (1d post last) the rmTBI 3d group exhibited increased edematous tissue (white arrowheads) at the site of the second impact, while a more heterogeneous lesion appeared at the site of the initial injury (Fig. 3A). However in rmTBI 7d animals, injury was composed primarily of blood at the site of the initial impact, while a larger injury of similar composition to that of a Single mTBI was observed at the site of second impact (white arrowheads; Fig. 3A). At the time of last MRI, little or no observable abnormalities were detected within the tissues (Fig. 3A). Volumetric 3D reconstruction of mTBI volumes illustrates the location and extent of the mild injury of our model revealing an increase in total lesion volume within rmTBI 7d animals compared to other groups (Fig. 3B).

Temporal mTBI injury volumes were further assessed to determine whether ongoing pathology from the first mTBI resulted in an exacerbation of lesion volume following a second mTBI (Fig. 3C). The rmTBI 7d group demonstrated a significantly increased lesion volume ($p = 0.018$) compared to other groups at 1d post last injury (Fig. 3C). The observed increases in the rmTBI 7d lesion volumes were transient with lesion volumes similar to those observed in other groups by 14d post first injury (Fig. 3C). We then further dichotomized the mTBI injury volume by examining independently the first and second lesion volumes to test whether differences existed between the first and second injuries. This analysis revealed a significant increase ($p = 0.029$) in lesion volume at the site of the second injury within rmTBI 7d animals 1d post last injury compared to Single animals, which was not observed in the rmTBI 3d group (Fig. 3D). The rmTBI injuries seen at the site of initial impact appeared similar to that observed in Single animals at 1d post last injury (Fig. 3D). By 14d post injury (first: 14d post first, second: 14d post last injury), significantly decreased lesion volumes were observed in all rmTBI animals compared to Singles (Fig. 3D).

3.3. Interval between rmTBI dictates injury characteristics: edema versus blood

Computational analyses of the first and second lesions were performed to determine the relative contribution of blood and edema (based on T2 values) at each injury site (Fig. 4). At 1d post last injury, computational analysis of the voxels containing blood (green), edema (red) and NAB (blue) at the injury sites clearly demonstrates that lesion within Single mTBI animals had a mixture of voxels containing blood, edema and NAB as was seen in the MRI (arrowheads; Fig. 4A). In contrast rmTBI 3d animals exhibited predominately edema (red) at the site of the second mTBI, as was observed in T2 MRI (hyper-intense signal; arrowheads). The site of the first injury within rmTBI 7d animals exhibited almost entirely blood (green) containing voxels, which can also be seen in T2 and SWI images (arrowheads; Fig. 4A).

Quantification of these voxel groups following a second impact in rmTBI 3d animals demonstrated a significant ($p = 0.038$) increase in the number of edema voxels (increased volume) 1d post last injury, which was dramatically resolved by 14d post injury (first: 14d post first, second: 14d post last injury) compared to Single animals (Fig. 4B). Further the rmTBI 3d group had a significantly ($p = 0.003$) greater edema volume than rmTBI 7d animals. The site of initial injury within the rmTBI 3d group also showed elevated edema volumes compared to other groups, though this was not significant (Fig. 4B). In contrast, the second injury in rmTBI 7d animals exhibited similar edema volumes to that observed after a Single mTBI, while the first lesion had a significant ($p = 0.001$) decrease in edematous tissue compared to the Single group at 1d post last injury (Fig. 4B).

Both injury sites of rmTBI 7d animals demonstrated a significant increase (1st: $p = 0.0001$; 2nd: $p = 0.025$) in blood volume compared to a Single mTBI at 1d post last injury (Fig. 4C). However, while there was an increase in the total amount of blood seen in the rmTBI 7d animals, the first and second blood volumes were not significantly different from each other. Further the rmTBI 7d group contained significantly more blood than the rmTBI 3d group ($p = 0.04$). The first lesion within rmTBI 3d animals had a similar blood volume to that seen after a Single mTBI 1d post injury, while the site of second injury had a smaller blood volume compared to other injury groups (Fig. 4C). Significant differences ($p = 0.047$) in blood volume were still observed 14d following the initial injury, while blood deposition at the site of the second mTBI appeared similar between the rmTBI groups at 14d post second injury (Fig. 4C).

Prussian blue staining for extravascular blood at the site of the lesions was performed 14d post first injury and supported our MRI analysis, demonstrating increased blood deposition within the rmTBI 7d animals compared to other groups (Fig. 4D). Blood deposition also appeared concentrated underneath the impact site within the Single and rmTBI

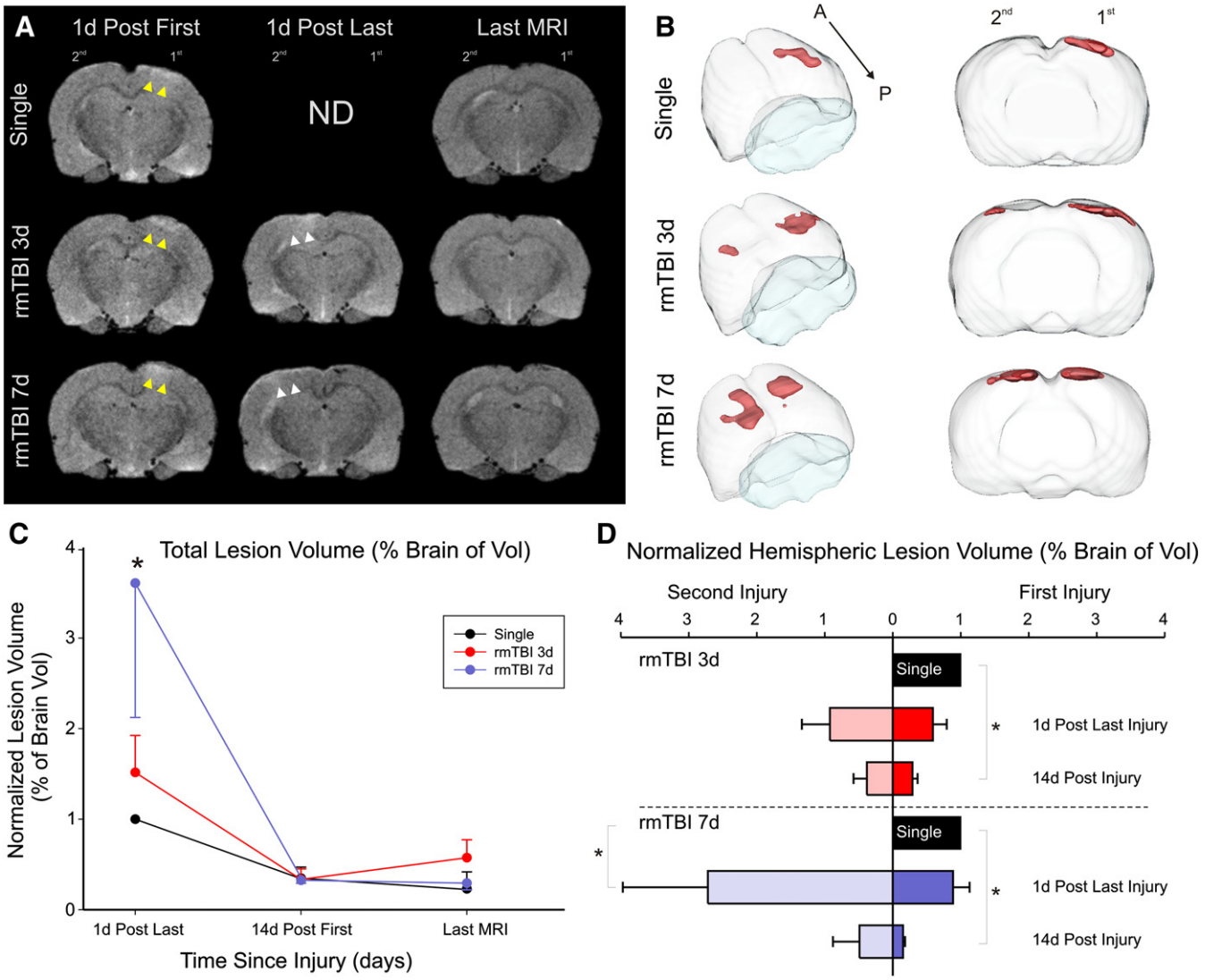

Fig. 3. rmTBI 7d animals have increased lesion volumes. A. Representative T2WIs illustrating the presence of abnormal tissue after the initial (1d post first; yellow arrows) and second (1d post last; white arrows) mTBI. B. 3D reconstruction of injury volumes illustrates the mild nature of the mTBI injury, where average total lesion volumes from Single (1.4%), rmTBI 3d (0.9%) and rmTBI 7d (2.0%) animals were collected 1d post last injury. C. The temporal evolution of total (first + second) mTBI lesion volumes over the experimental period, demonstrates a significantly increased lesion volume in rmTBI 7d animals 1d post last injury compared to other groups. D. Evaluation of the first and second injuries revealed a transient increase ($p = 0.029$) in the second lesion volume of rmTBI 7d animals compared to Singles 1d post last injury. Normalized data presented as means ± SEM, where $^{*}p < 0.05$.

3d groups, while the rmTBI 7d animals had a more diffuse deposition (see below, Fig. 4D).

3.4. Activated microglia demonstrates spatial overlap with blood deposition

We undertook an analysis of the distribution of Prussian blue staining (blood) at 14d post first injury (Fig. 5), where we observed a modest increase in the blood containing area at the site of the first impact in rmTBI 7d animals (Fig. 5A). In contrast, the site of the second injury in rmTBI 3d animals revealed blood deposition primarily underneath the impact site, while rmTBI 7d animals demonstrated a dramatic increase in width and depth of blood (Fig. 5A), often down to the corpus callosum.

Measurements of activated microglia (IBA1) containing regions revealed a similar profile with locations encompassing blood deposition (Fig. 5A). The site of initial injury demonstrated a smaller area of microglial activation compared to blood containing zones in both rmTBI 3d and Single groups, while regions were approximately the same size in rmTBI 7d animals (Fig. 5A). In contrast, the site of second injury in both rmTBI groups had an increased dispersion of microglial activation beyond the regions containing blood, which was most prominent within the rmTBI 7d group (Fig. 5A). Staining for astrocytes (GFAP) revealed increased reactivity only at the site of second injury within rmTBI groups, which was confined to the immediate vicinity of the impact site (data not shown).

A modest number of Fluoro-Jade positive cell-bodies were observed at the site of the second impact in rmTBI 7d animals suggesting some ongoing neuronal degeneration, which was not seen in the first injury site or in other groups (data not shown). However in all mTBI groups punctate staining was observed, reminiscent of axonal or dendritic debris, at the site of the first injury but not in the left non-injured cortex of Single animals suggesting ongoing microstructural damage (data not shown).

4. Discussion

Using a novel computational approach we report the temporal detection and quantification of blood and edema for the first time, providing new insight into the progression of neuropathology following

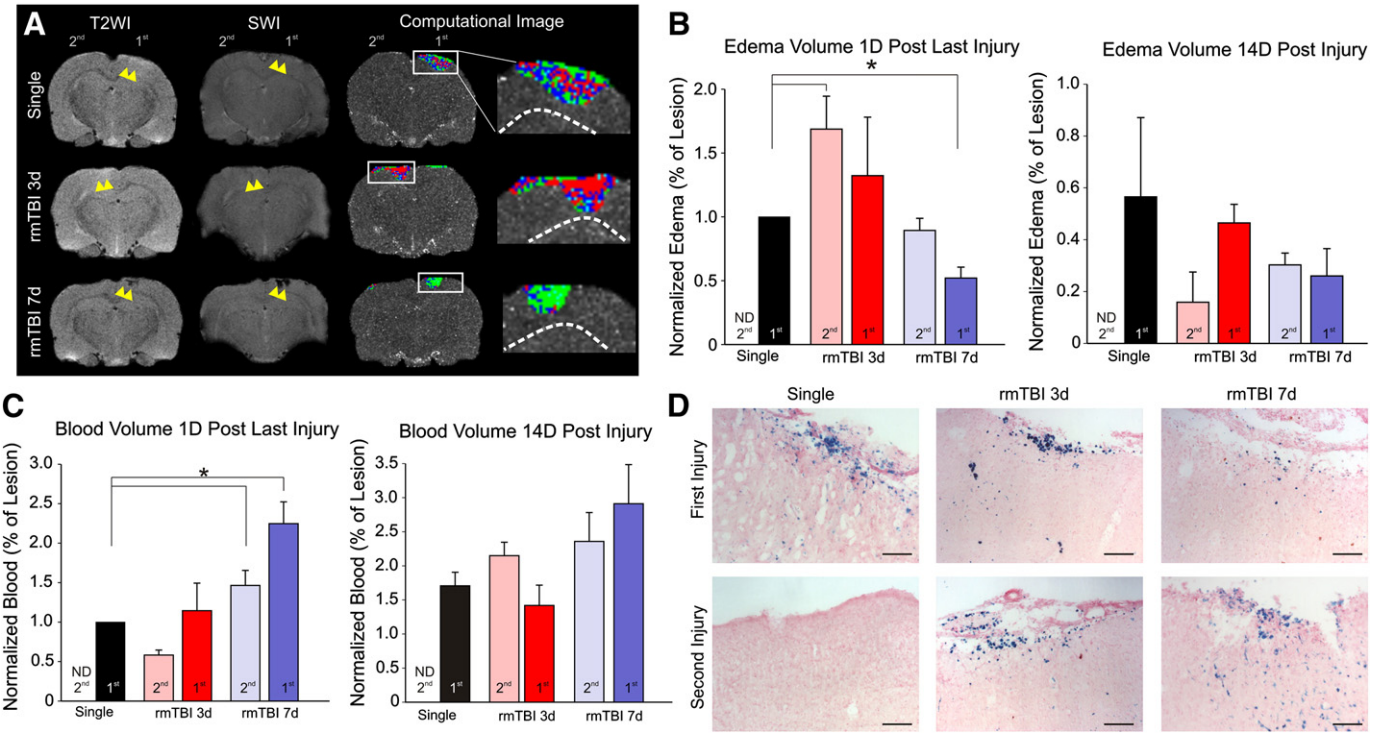

Fig. 4. Voxel-wise analysis reveals increased blood volume in the rmTBI 7d animals. A. MRI taken 1d post last injury reveals abnormal tissue on T2 (yellow arrows) and blood deposition on SWI (yellow arrows) following mTBI. Computationally color-coded images illustrate voxel characterization (green = blood, red = edema, blue = normal appearing brain) in these animals. B. Edema volume analysis within the first and second lesions revealed changes in edematous tissue at 1d post last injury, while no differences were observed between groups at 14d post injury (first: 14d post first, second: 14d post last injury). C. Analysis of blood volume within the first and second lesions demonstrated significantly increased blood deposition within rmTBI 7d animals at 1d post last injury and between the first lesions at 14d post injury (first: 14d post first, second: 14d post last injury). D. Prussian blue staining in the first and second lesions of animals 14d post first injury at the site of maximal lesion shows increased blood deposition in the tissues from rmTBI 7d animals. Normalized graphs presented as means ± SEM where $^{*}p<0.05$; cal bar = 100 μm.

a unique model of rmTBI. Our novel findings include: 1) T2 histogram evidence of increased edematous tissue in rmTBI 3d animals and increased blood deposition in rmTBI 7d animals. 2) Increased lesion volume within rmTBI 7d animals, which was not observed in the rmTBI 3d animals. 3) Hemorrhagic progression of the lesion was detected, using a voxel-wise comparison, within the lesion of rmTBI 7d animals, while increased edematous tissue was observed in rmTBI 3d animals. 4) Prussian blue staining confirmed the presence and revealed the spatial distribution of blood within the cortex 14d post first injury. 5) At the site of the second injury, an increased inflammatory response was detected in both rmTBI groups, while ongoing neuronal death was only observed in rmTBI 7d animals. Taken together, our study further demonstrates that there are differential increases in tissue vulnerability following rmTBI and that the underlying pathology is dependent upon the interval between and location of mTBI events.

4.1. Lesion histograms predict temporal changes in rmTBI pathology

Initially, we used voxel-wise T2 histograms to analyze rmTBI lesions to evaluate global temporal changes in tissue pathology. This is the first report using T2-histograms in an experimental model of mTBI, as there are no previous publications to our knowledge. In contrast, other clinical studies and animal models of central nervous system (CNS) injuries including tumors, spinal cord injury and ischemia, have used histogram analysis (Emblem et al., 2008; Kopelman et al., 2005; Nevo et al., 2001; Veltkamp et al., 2005).

Clinically, histograms have also been employed to quickly assess whole brain and tissue-specific (white and gray matter) MRI changes in mild to severe TBI (Lipton et al., 2008; Marquez de la Plata et al., 2011; Shanmuganathan et al., 2004). While histogram analysis has demonstrated some ambiguity in sensitivity from clinical data others have reported its effectiveness to discriminate TBI. Whole-brain histograms in mTBI patients undergoing diffusion tensor imaging (DTI) found no differences in the mean diffusivity (MD) and fractional anisotropy (FA) measurements between injured and control patients (Inglese et al., 2005). However when the histogram analysis was focused to ROIs drawn within white matter tracts susceptible to mTBI, increased MD and decreased FA were observed in injured patients (Inglese et al., 2005). In contrast, application of global histograms (whole white matter) from DTI images were able to identify mTBI, reporting decreased FA without the need for ROIs (Benson et al., 2007). These clinical studies suggest that histograms have the potential to detect subtle tissue changes associated with mild injuries when analysis is focused on specific brain regions rather than performing whole-brain histogram analysis. In our study we observed temporal histogram skewness and kurtosis changes within defined mTBI lesions, suggesting tissue heterogeneity associated with edema resolution and ongoing blood deposition. These findings confirm that histogram analysis has the potential

Fig. 5. Microglial activation and blood deposition demonstrate spatial overlap within the lesion sites. A. A depiction of the rat cortex illustrates the locations of observable tissue damage where blood and microglial measurements were taken. Depth and width graphs demonstrate a spatial overlap in the blood and activated microglial localization at 14d post first injury. Single data in the second injury (dotted line) is from the injured cortex (first injury) for comparison. B. Representative Prussian blue and IBA1 images, taken from adjacent sections of rmTBI 7d (second injury) and Single (first injury) animals, show the localization of blood and activated microglia within the cortices. cal bar = 100 μm; inset cal bar = 20 μm.

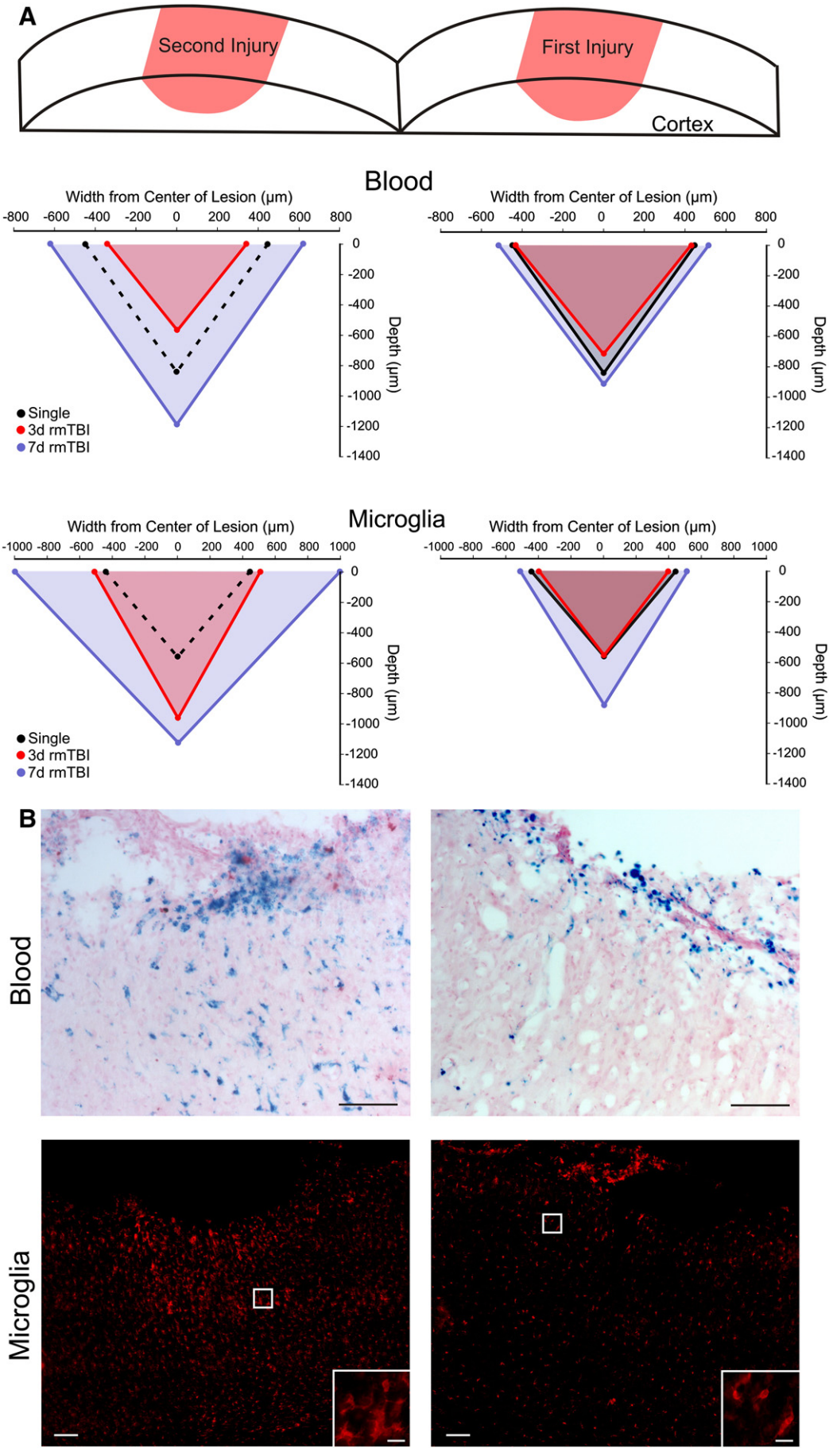
A
Second Injury
First Injury
Cortex
Blood
Width from Center of Lesion (μm)
-800 -600 -400 -200 0 200 400 600 800
0 -200 -400 -600 -800 -1000 -1200 -1400
Depth (μm)
Single
3d rmTBI
7d rmTBI
Microglia
-1000 -800 -600 -400 -200 0 200 400 600 800 1000
B
Blood
Microglia

to discriminate between the mTBI groups as the lesions progress and resolve over time. Our results set a foundation for future comparisons of whole brain and regional histogram analysis so that additional methods can be developed for efficient and accurate comparisons of clinically defined mTBI.

4.2. Exacerbation of rmTBI lesion volume is dependent on the time interval between injuries

We found that tissue damage was exacerbated following a second mTBI, particularly, when the injuries were 7d apart. The increased lesion volume was predominantly due to exacerbated tissue damage at the site of the second injury. This suggests that a Single mTBI can affect distant brain regions in such a way that they remain vulnerable to a subsequent injury.

The neuropathology and long-term consequences of rmTBI are not well understood. Rodent models of experimental rmTBI have demonstrated that there exists a window of vulnerability in which two injuries can result in exacerbated tissue damage (Longhi et al., 2005; Vagnozzi et al., 2007). Animals sustaining mTBIs 3 or 5 days apart on the same hemisphere exhibited increased cognitive deficits for up to a week following injury and cell death and axonal disruption 72 h following the last injury (Longhi et al., 2005). Similarly, an examination of changes in energy metabolism using MR spectroscopy, demonstrated the greatest changes following mTBIs sustained 3d apart and which persisted for up to a week (Vagnozzi et al., 2007). However, the changes observed by Longhi et al. (2005) were not observed in animals receiving two impacts 7 days apart, while alterations in metabolism described by Vagnozzi et al. (2007) were not observed in animals sustaining injuries 5 days apart. Collectively, these studies suggest that by >5 days the tissue has had enough time to heal and so a second impact was similar to sustaining a Single mTBI when delivered to the same hemisphere. Additional rmTBI studies inducing two impacts 24 h apart have further supported these findings, where in the absence of gross histological abnormalities, increased neurological deficits were persistent for several weeks with an acute increase in axonal injury and increased inflammation (Laurer et al., 2001; Shitaka et al., 2011).

However these models induced rmTBI to the same anatomical location, while our model induces mTBI injuries distant from each other. This suggests that brain vulnerability is dependent on not only the interval between injuries but also the location where the injuries are sustained. Patients sustaining an mTBI demonstrated metabolic tissue deficits for approximately 1 month following injury while those sustaining a second mTBI within 10–13 days of the first demonstrated a prolonged alteration (Vagnozzi et al., 2008). While perhaps brain regions close to each other may have a shorter window of vulnerability, locations farther apart appear to have a delayed or lengthened period of vulnerability.

4.3. HPC primarily contributes to the lesion volume of rmTBI 7d animals

Computational analysis of blood and edema contribution to the abnormal tissue volume revealed that rmTBI 3d animals had increased edema volumes, while the rmTBI 7d group exhibited increased blood deposition. By 14d post injury (14d post first and 14d post last injury) the lesions of both rmTBI groups appeared to have a persistent increase in blood deposition, while edema resolved. It is important to note that extravascular blood can demonstrate a temporal change in MRI signature, as observed in an animal model of intracranial hemorrhage (ICH) (Belayev et al., 2007). However due to the mild nature of our TBI model and the ongoing blood deposition, as a result of hemorrhagic progression, we would expect a different temporal course of extravascular blood deposition than that observed following ICH.

Our findings of increased blood deposition with time concurs with the concept of hemorrhagic progression of the contusion (HPC), which has been modeled experimentally in moderate to severe traumatic brain and spinal cord injury (Gerzanich et al., 2009; Simard et al., 2009). Within 12 h of a moderate to severe TBI, HPC was observed where the blood volume expanded (2 fold) into the hippocampus and thalamus (Simard et al., 2009). Similarly, in our rmTBI 7d model, at 1d post last injury we observed a 2.5 fold increase in blood volume at the site of the initial injury in the rmTBI 7d group. Several studies have demonstrated concordance between Prussian blue staining of tissue iron deposition and T2 weighted MRI (Belayev et al., 2007; Gupta et al., 2012; Thulborn et al., 1990). Our histological staining for extravascular blood further supported the expansion of bleeding in the rmTBI 7d animals, which was not observed in other mTBI groups nor has been reported in other models of rmTBI.

Models of CNS injury have identified the sulfonylurea receptor1-regulated $NC_{Ca\text{-}ATP}$ channel (SUR1/TRPM4) as a key mediator in the development of HPC (Gerzanich et al., 2009; Simard et al., 2009). These molecules are upregulated following trauma and upon depletion of ATP, a deregulation of this channel occurs leading to capillary fragmentation and hemorrhage (Simard et al., 2010). HPC in our model was identified using temporal MRI at acute time points and Prussian blue staining at sub-acute times following injury. Our tissue was collected at late time points, thus we could not identify the cellular cascades, which occur within hours to days following trauma (Simard et al., 2009).

Clinically, HPC has been identified using CT, where approximately 45–50% of patients develop this pathology following a mild to severe TBI (Alahmadi et al., 2010; Narayan et al., 2008; Sifri et al., 2004, 2006). A clinical study quantifying changes in hematoma size, using CT following a TBI (mild to severe), found that 4% shrank, 58% were unchanged and 38% increased in volume within 72 h (Chang et al., 2006). Clinical evidence of HPC suggests that medical imaging can be used to identify this pathology, though future experimental studies of the underlying cascades need to be performed to validate and better understand the underlying HPC mechanisms.

Another potential mechanism for our observed increase in blood volume could be due to extracellular matrix remodeling and subsequent revascularization of the tissue. In models of ischemic stroke, hemorrhagic transformation has been observed and associated with breakdown of the extracellular matrix (ECM), which contributes to microvascular integrity (Fukuda et al., 2004; Hamann et al., 1995). Metalloproteinases (MMP) have been shown to be associated with microvessel ECM degradation and blood brain barrier permeability following experimental models of stroke (Fukuda et al., 2004; Gidday et al., 2005). In models of moderate to severe TBI, MMPs are upregulated with maximal levels being reached at 24 h and can remain high for up to 7 days following injury (Hayashi et al., 2009; Wang et al., 2000). In cell culture models of ischemia, microglia increased secretion of the inactive form of MMP-9, which in non-human primate models of stroke demonstrated a linear relationship with blood deposition (Del Zoppo et al., 2012). Treatment of moderate TBI with Minocycline, a drug shown to suppress microglial activation, inhibited MMPs and resulted in increased synaptic preservation (Ding et al., 2009). Additionally, knockout of MMP-9 demonstrated decreased lesion volumes and improved neurological outcomes following moderate TBI compared to control mice (Wang et al., 2000). Future examination could include tissue collected at these early time points for changes in the ECM as a result of MMPs. Collectively these studies demonstrate that MMPs play a role in tissue exacerbation following trauma though their role in HPC is not clear.

4.4. Increased neuroinflammation at the site of the second injury in rmTBI animals

Extravascular blood within brain tissues can result in apoptosis and initiate a neuroinflammatory response, including peripheral leukocyte infiltration and microglial activation (Gong et al., 2000; Xue and Del

Bigio, 2000). We found that there was a distinct overlap of brain regions containing activated microglia and extravascular blood, although microglial responses encompassed a slightly larger area at the site of the second impact, particularly in the rmTBI 7d group. Microglia have been identified as potential aggravators of CNS tissue damage. During CNS infection or injury classically activated microglia release reactive oxygen species causing further tissue damage, but suppression of microglia demonstrates decreased TBI related tissue loss (Boje and Arora, 1992; Homsi et al., 2009). A study of the inflammatory response to microhemorrhages within brain tissue found that microglia within 200 μm of blood can remain responsive for up to 7 days (Rosidi et al., 2011). Our observed increase in microglial response and its detrimental effects is consistent with increased lesion volumes observed at the site of second injury within rmTBI 7d animals.

4.5. Conclusions

Our new model of rmTBI, in which injuries were induced to opposite hemispheres, demonstrated that there exists a window of tissue vulnerability following an initial mTBI. We previously hypothesized that animals receiving impacts 7d apart would not exhibit increased tissue damage, while injuries sustained 3d apart would result in larger lesion volumes specifically at the site of the second injury. However, our data supports that this temporal window occurs at a later time point than previously described (7d vs. 3d) and is likely the result of the second injury location being distant from the first. Analysis of cortical abnormalities using our rapid computational approach revealed increased blood deposition within rmTBI 7d animals consistent with HPC, which was not observed in the rmTBI 3d group. This increased blood deposition was also observed to co-localize with regions of activated microglia, which may further cause tissue damage at regions distant from the impact site leading to the increased lesion volumes observed in rmTBI 7d animals. The vulnerability to a second impact resulted in both a greater volume of tissue damage and increased blood deposition following a second temporally and spatially distant mTBI. The differences in observed blood and edema volumes between the rmTBI groups are most likely the result of temporal cellular cascades, such as HPC, initiated by an initial injury. However additional investigations are needed to uncover the mechanisms leading to increased brain vulnerability and blood deposition within rmTBI 7d animals and determine the long-term effects of this observed tissue exacerbation. Further computational analysis methods need to be developed for experimental models of TBI so that they can be optimized for future clinical use.

Acknowledgments

This study was supported by funding from Department of Defense (DCMRP #DR080470 to AO) and in part by National Science Foundation Integrative Graduate Education and Research Traineeship (IGERT) in Video Bioinformatics (DGE 0903667 to VD, AB and BB).

The authors wish to acknowledge the Center for Glial-Neuronal Interactions and thank Kamalakar Ambadipudi and Sonny Kim for imaging assistance. Additionally, the authors would like to thank Jacqueline Coats and Alena Mohd-Yussof for assistance in performing surgeries and drawing regions of interest.

References

Alahmadi, H., Vachhrajani, S., Cusimano, M.D., 2010. The natural history of brain contusion: an analysis of radiological and clinical progression. Journal of Neurosurgery 112, 1139–1145.

Belanger, H.G., Spiegel, E., Vanderploeg, R.D., 2010. Neuropsychological performance following a history of multiple self-reported concussions: a meta-analysis. Journal of International Neuropsychological Society 16, 262–267.

Belayev, L., Obenaus, A., Zhao, W., Saul, I., Busto, R., Wu, C., Vigdorchik, A., Lin, B., Ginsberg, M.D., 2007. Experimental intracerebral hematoma in the rat: characterization by sequential magnetic resonance imaging, behavior, and histopathology. Effect of albumin therapy. Brain Research 1157, 146–155.

Benson, R.R., Meda, S.A., Vasudevan, S., Kou, Z., Govindarajan, K.A., Hanks, R.A., Millis, S.R., Makki, M., Latif, Z., Coplin, W., Meythaler, J., Haacke, E.M., 2007. Global white matter analysis of diffusion tensor images is predictive of injury severity in traumatic brain injury. Journal of Neurotrauma 24, 446–459.

Boje, K.M., Arora, P.K., 1992. Microglial-produced nitric oxide and reactive nitrogen oxides mediate neuronal cell death. Brain Research 587, 250–256.

Chang, E.F., Meeker, M., Holland, M.C., 2006. Acute traumatic intraparenchymal hemorrhage: risk factors for progression in the early post-injury period. Neurosurgery 58, 647–656 discussion 647–656.

Colgan, N.C., Cronin, M.M., Gobbo, O.L., O'Mara, S.M., O'Connor, W.T., Gilchrist, M.D., 2010. Quantitative MRI analysis of brain volume changes due to controlled cortical impact. Journal of Neurotrauma 27, 1265–1274.

Corrigan, J.D., Selassie, A.W., Orman, J.A., 2010. The epidemiology of traumatic brain injury. The Journal of Head Trauma Rehabilitation 25, 72–80.

DeFord, S.M., Wilson, M.S., Rice, A.C., Clausen, T., Rice, L.K., Barabnova, A., Bullock, R., Hamm, R.J., 2002. Repeated mild brain injuries result in cognitive impairment in B6C3F1 mice. Journal of Neurotrauma 19, 427–438.

Del Zoppo, G.J., Frankowski, H., Gu, Y.H., Osada, T., Kanazawa, M., Milner, R., Wang, X., Hosomi, N., Mabuchi, T., Koziol, J.A., 2012. Microglial cell activation is a source of metalloproteinase generation during hemorrhagic transformation. Journal of Cerebral Blood Flow and Metabolism 32, 919–932.

Ding, J.Y., Kreipke, C.W., Schafer, P., Schafer, S., Speirs, S.L., Rafols, J.A., 2009. Synapse loss regulated by matrix metalloproteinases in traumatic brain injury is associated with hypoxia inducible factor-1alpha expression. Brain Research 1268, 125–134.

Emblem, K.E., Scheie, D., Due-Tonnessen, P., Nedregaard, B., Nome, T., Hald, J.K., Beiske, K., Meling, T.R., Bjornerud, A., 2008. Histogram analysis of MR imaging-derived cerebral blood volume maps: combined glioma grading and identification of low-grade oligodendroglial subtypes. AJNR American Journal of Neuroradiology 29, 1664–1670.

Faul, M., Xu, L., Wald, M.M., Coronado, V.G., 2010. Traumatic Brain Injury in the United States: Emergency Department Visits, Hospitalizations and Deaths. Centers for Disease Control and Prevention National Center for Injury Prevention and Control, Atlanta, GA.

Fukuda, S., Fini, C.A., Mabuchi, T., Koziol, J.A., Eggleston Jr., L.L., del Zoppo, G.J., 2004. Focal cerebral ischemia induces active proteases that degrade microvascular matrix. Stroke 35, 998–1004.

Gerzanich, V., Woo, S.K., Vennekens, R., Tsymbalyuk, O., Ivanova, S., Ivanov, A., Geng, Z., Chen, Z., Nilius, B., Flockerzi, V., Freichel, M., Simard, J.M., 2009. De novo expression of Trpm4 initiates secondary hemorrhage in spinal cord injury. Nature Medicine 15, 185–191.

Gidday, J.M., Gasche, Y.G., Copin, J.C., Shah, A.R., Perez, R.S., Shapiro, S.D., Chan, P.H., Park, T.S., 2005. Leukocyte-derived matrix metalloproteinase-9 mediates blood–brain barrier breakdown and is proinflammatory after transient focal cerebral ischemia. American Journal of Physiology — Heart and Circulatory Physiology 289, H558–568.

Gong, C., Hoff, J.T., Keep, R.F., 2000. Acute inflammatory reaction following experimental intracerebral hemorrhage in rat. Brain Research 871, 57–65.

Gupta, R.K., Tomar, V., Awasthi, R., Yadav, A., Husain, N., Bharadwaj, V., Ojha, B.K., Behari, S., Prasad, K.N., Rathore, R.K., 2012. T2*-weighted MR angiography substantially increases the detection of hemorrhage in the wall of brain abscess: implications in clinical interpretation. Neuroradiology 54, 565–572.

Hamann, G.F., Okada, Y., Fitridge, R., del Zoppo, G.J., 1995. Microvascular basal lamina antigens disappear during cerebral ischemia and reperfusion. Stroke 26, 2120–2126.

Hayashi, T., Kaneko, Y., Yu, S., Bae, E., Stahl, C.E., Kawase, T., van Loveren, H., Sanberg, P.R., Borlongan, C.V., 2009. Quantitative analyses of matrix metalloproteinase activity after traumatic brain injury in adult rats. Brain Research 1280, 172–177.

Homsi, S., Federico, F., Croci, N., Palmier, B., Plotkine, M., Marchand-Leroux, C., Jafarian-Tehrani, M., 2009. Minocycline effects on cerebral edema: relations with inflammatory and oxidative stress markers following traumatic brain injury in mice. Brain Research 1291, 122–132.

Immonen, R.J., Kharatishvili, I., Grohn, H., Pitkanen, A., Grohn, O.H., 2009. Quantitative MRI predicts long-term structural and functional outcome after experimental traumatic brain injury. NeuroImage 45, 1–9.

Inglese, M., Makani, S., Johnson, G., Cohen, B.A., Silver, J.A., Gonen, O., Grossman, R.I., 2005. Diffuse axonal injury in mild traumatic brain injury: a diffusion tensor imaging study. Journal of Neurosurgery 103, 298–303.

Irimia, A., Chambers, M.C., Alger, J.R., Filippou, M., Prastawa, M.W., Wang, B., Hovda, D.A., Gerig, G., Toga, A.W., Kikinis, R., Vespa, P.M., Van Horn, J.D., 2011. Comparison of acute and chronic traumatic brain injury using semi-automatic multimodal segmentation of MR volumes. Journal of Neurotrauma 28, 2287–2306.

Kane, M.J., Angoa-Perez, M., Briggs, D.I., Viano, D.C., Kreipke, C.W., Kuhn, D.M., 2012. A mouse model of human repetitive mild traumatic brain injury. Journal of Neuroscience Methods 203, 41–49.

Kharatishvili, I., Sierra, A., Immonen, R.J., Grohn, O.H., Pitkanen, A., 2009. Quantitative T2 mapping as a potential marker for the initial assessment of the severity of damage after traumatic brain injury in rat. Experimental Neurology 217, 154–164.

Kopelman, R., Lee, Y.K., Philbert, M., Moffat, B.A., Reddy, G.R., McConville, P., Hall, D., Chenevert, T.L., Bhojani, T.L., Buck, S.M., Rehemtulla, A., Ross, B.D., 2005. Multifunctional nanoparticle platforms for in vivo MRI enhancement and photodynamic therapy of a rat brain cancer. Journal of Magnetism and Magnetic Materials 293, 404–410.

Kurland, D., Hong, C., Aarabi, B., Gerzanich, V., Simard, J.M., 2012. Hemorrhagic progression of a contusion after traumatic brain injury: a review. Journal of Neurotrauma 29, 19–31.

Laurer, H.L., Bareyre, F.M., Lee, V.M., Trojanowski, J.Q., Longhi, L., Hoover, R., Saatman, K.E., Raghupathi, R., Hoshino, S., Grady, M.S., McIntosh, T.K., 2001. Mild head injury increasing the brain's vulnerability to a second concussive impact. Journal of Neurosurgery 95, 859–870.

Lee, H., Wintermark, M., Gean, A.D., Ghajar, J., Manley, G.T., Mukherjee, P., 2008. Focal lesions in acute mild traumatic brain injury and neurocognitive outcome: CT versus 3T MRI. Journal of Neurotrauma 25, 1049–1056.

Lipton, M.L., Gellella, E., Lo, C., Gold, T., Ardekani, B.A., Shifteh, K., Bello, J.A., Branch, C.A., 2008. Multifocal white matter ultrastructural abnormalities in mild traumatic brain injury with cognitive disability: a voxel-wise analysis of diffusion tensor imaging. Journal of Neurotrauma 25, 1335–1342.

Longhi, L., Saatman, K.E., Fujimoto, S., Raghupathi, R., Meaney, D.F., Davis, J., McMillan, B.S.A., Conte, V., Laurer, H.L., Stein, S., Stocchetti, N., McIntosh, T.K., 2005. Temporal window of vulnerability to repetitive experimental concussive brain injury. Neurosurgery 56, 364–374 discussion 364–374.

Marquez de la Plata, C.D., Yang, F.G., Wang, J.Y., Krishnan, K., Bakhadirov, K., Paliotta, C., Aslan, S., Devous, M.D., Moore, C., Harper, C., McColl, R., Munro Cullum, C., Diaz-Arrastia, R., 2011. Diffusion tensor imaging biomarkers for traumatic axonal injury: analysis of three analytic methods. Journal of International Neuropsychological Society 17, 24–35.

Narayan, R.K., Maas, A.I., Servadei, F., Skolnick, B.E., Tillinger, M.N., Marshall, L.F., 2008. Progression of traumatic intracerebral hemorrhage: a prospective observational study. Journal of Neurotrauma 25, 629–639.

Nevo, U., Hauben, E., Yoles, E., Agranov, E., Akselrod, S., Schwartz, M., Neeman, M., 2001. Diffusion anisotropy MRI for quantitative assessment of recovery in injured rat spinal cord. Magnetic Resonance in Medicine 45, 1–9.

Obenaus, A., Dilmac, N., Tone, B., Tian, H.R., Hartman, R., Digicaylioglu, M., Snyder, E.Y., Ashwal, S., 2011. Long-term magnetic resonance imaging of stem cells in neonatal ischemic injury. Annals of Neurology 69, 282–291.

Obenaus, A., Huang, L., Smith, A., Favre, C.J., Nelson, G., Kendall, E., 2008. Magnetic resonance imaging and spectroscopy of the rat hippocampus 1 month after exposure to 56Fe-particle radiation. Radiation Research 169, 149–161.

Obenaus, A., Robbins, M., Blanco, G., Galloway, N.R., Snissarenko, E., Gillard, E., Lee, S., Curras-Collazo, M., 2007. Multi-modal magnetic resonance imaging alterations in two rat models of mild neurotrauma. Journal of Neurotrauma 24, 1147–1160.

Oehmichen, M., Walter, T., Meissner, C., Friedrich, H.J., 2003. Time course of cortical hemorrhages after closed traumatic brain injury: statistical analysis of posttraumatic histomorphological alterations. Journal of Neurotrauma 20, 87–103.

Rosidi, N.L., Zhou, J., Pattanaik, S., Wang, P., Jin, W., Brophy, M., Olbricht, W.L., Nishimura, N., Schaffer, C.B., 2011. Cortical microhemorrhages cause local inflammation but do not trigger widespread dendrite degeneration. PLoS One 6, e26612.

Schmued, L.C., Hopkins, K.J., 2000. Fluoro-Jade: novel fluorochromes for detecting toxicant-induced neuronal degeneration. Toxicologic Pathology 28, 91–99.

Shanmuganathan, K., Gullapalli, R.P., Mirvis, S.E., Roys, S., Murthy, P., 2004. Whole-brain apparent diffusion coefficient in traumatic brain injury: correlation with Glasgow Coma Scale score. AJNR. American Journal of Neuroradiology 25, 539–544.

Shitaka, Y., Tran, H.T., Bennett, R.E., Sanchez, L., Levy, M.A., Dikranian, K., Brody, D.L., 2011. Repetitive closed-skull traumatic brain injury in mice causes persistent multifocal axonal injury and microglial reactivity. Journal of Neuropathology and Experimental Neurology 70, 551–567.

Shultz, S.R., Bao, F., Omana, V., Chiu, C., Brown, A., Cain, D.P., 2012. Repeated mild lateral fluid percussion brain injury in the rat causes cumulative long-term behavioral impairments, neuroinflammation, and cortical loss in an animal model of repeated concussion. Journal of Neurotrauma 29, 281–294.

Sifri, Z.C., Homnick, A.T., Vaynman, A., Lavery, R., Liao, W., Mohr, A., Hauser, C.J., Manniker, A., Livingston, D., 2006. A prospective evaluation of the value of repeat cranial computed tomography in patients with minimal head injury and an intracranial bleed. The Journal of Trauma 61, 862–867.

Sifri, Z.C., Livingston, D.H., Lavery, R.F., Homnick, A.T., Mosenthal, A.C., Mohr, A.M., Hauser, C.J., 2004. Value of repeat cranial computed axial tomography scanning in patients with minimal head injury. American Journal of Surgery 187, 338–342.

Simard, J.M., Kahle, K.T., Gerzanich, V., 2010. Molecular mechanisms of microvascular failure in central nervous system injury — synergistic roles of NKCC1 and SUR1/TRPM4. Journal of Neurosurgery 113, 622–629.

Simard, J.M., Kilbourne, M., Tsymbalyuk, O., Tosun, C., Caridi, J., Ivanova, S., Keledjian, K., Bochicchio, G., Gerzanich, V., 2009. Key role of sulfonylurea receptor 1 in progressive secondary hemorrhage after brain contusion. Journal of Neurotrauma 26, 2257–2267.

Tagliaferri, F., Compagnone, C., Korsic, M., Servadei, F., Kraus, J., 2006. A systematic review of brain injury epidemiology in Europe. Acta Neurochirurgica 148, 255–268 discussion 268.

Thulborn, K.R., Sorensen, A.G., Kowall, N.W., McKee, A., Lai, A., McKinstry, R.C., Moore, J., Rosen, B.R., Brady, T.J., 1990. The role of ferritin and hemosiderin in the MR appearance of cerebral hemorrhage: a histopathologic biochemical study in rats. AJR. American Journal of Roentgenology 154, 1053–1059.

VA/DoD, 2009. Management of concussion/mild traumatic brain injury. VA/DoD Evidence Based Practice: Clinical Practice Guideline.

Vagnozzi, R., Signoretti, S., Tavazzi, B., Floris, R., Ludovici, A., Marziali, S., Tarascio, G., Amorini, A.M., Di Pietro, V., Delfini, R., Lazzarino, G., 2008. Temporal window of metabolic brain vulnerability to concussion: a pilot 1H-magnetic resonance spectroscopic study in concussed athletes—part III. Neurosurgery 62, 1286–1295 discussion 1295–1286.

Vagnozzi, R., Tavazzi, B., Signoretti, S., Amorini, A.M., Belli, A., Cimatti, M., Delfini, R., Di Pietro, V., Finocchiaro, A., Lazzarino, G., 2007. Temporal window of metabolic brain vulnerability to concussions: mitochondrial-related impairment—part I. Neurosurgery 61, 379–388 discussion 388–379.

Veltkamp, R., Siebing, D.A., Heiland, S., Schoenffeldt-Varas, P., Veltkamp, C., Schwaninger, M., Schwab, S., 2005. Hyperbaric oxygen induces rapid protection against focal cerebral ischemia. Brain Research 1037, 134–138.

Wang, X., Jung, J., Asahi, M., Chwang, W., Russo, L., Moskowitz, M.A., Dixon, C.E., Fini, M.E., Lo, E.H., 2000. Effects of matrix metalloproteinase-9 gene knock-out on morphological and motor outcomes after traumatic brain injury. Journal of Neuroscience 20, 7037–7042.

Xue, M., Del Bigio, M.R., 2000. Intracerebral injection of autologous whole blood in rats: time course of inflammation and cell death. Neuroscience Letters 283, 230–232.